Improved dielectric performance of polypropylene/multi-walled carbon nanotubes nanocomposites by solid phase orientation

Xiang Lin [a], Jie-Wei Tian [a], Peng-Hao Hu [a], Rohan Ambardekar [b], Glen Thompson [b], Zhi-Min Dang [a], Phil Coates [b]

[a] *Department of Polymer Science & Engineering, School of Chemistry and Biological Engineering, University of Science & Technology Beijing, Beijing, 100083, China*

[b] *IRC in Polymer Engineering, School of Engineering, Design & Technology, University of Bradford, Bradford BD7 1DP, West Yorkshire, United Kingdom*

***Corresponding to:** (1) Tel/Fax: +86106233 4516, E-mail address: huph@ustb.edu.cn (Prof. Penghao Hu).*

Abstract: By means of die drawing technique at rubber-state, effect of the orientation of microstructure on dielectric properties of polypropylene/multi-walled carbon nanotubes nanocomposites (PP/MWCNTs) was emphasized in this work. Viscoelasticity behavior of PP/MWCNTs with MWCNTs weight loadings from 0.25 to 5 wt% and dielectric performance of the stretched PP/MWCNTs under different drawing speeds and drawing ratios were studied for seeking an insight of the influences of dispersion and orientation state of MWCNTs and matrix molecular chains. A viscosity decrease (*ca.* 30%) of the PP/MWCNTs-0.25wt% melt was obviously observed owing to the free volume effect. Differential scanning calorimetry (DSC) and wide angle X-ray diffraction (WAXD) were adopted to detect the orientation structure and the variation of crystal morphology of PP/MWCNTs. Melting plateau regions, which indicated the mixed crystallization morphology for the stretched samples, were found in the DSC patterns instead of a single-peak for the unstretched samples. It was found that the uniaxial stretching process broke the conductive

MWCNTs networks and consequently increased the orientation of MWCNTs as well as molecular chains along the tensile force direction, leading to an improvement of the dielectric performance.

Keywords: Polypropylene; Viscosity and viscoelasticity; Dielectric properties; Nanocomposites; Solid phase orientation.

1. Introduction

By introducing of a small loading of conductive or semi-conductive nanoparticles into polymer matrix near the percolation threshold can result in a significant increase of dielectric constant (ε) without losing flexibility and mechanical strength [1-4]. Most of these nanocomposites are aiming to develop the novel application in wave absorption or heat-electric transition [5], but the high tanδ still confines the applications in the other fields. The present challenge always relies on the reducing the dielectric loss (tanδ) by designing the internal microstructure. How to prepare composites with high dielectric constant and low loss tangent is a topic of great interest. Based on this respect, improved dielectric performance of nanocomposites can be obtained by artificially modulating the internal microstructure, such as to improve the dispersion state of nanoparticles, to enhance the orientation degree of molecular chains as well as nanofibers and the interfacial morphology between matrix and additives, etc. Two routines are mostly adopted for achieving this destination: one is aiming to modify the polymeric chains as well as nanoparticles or to improve the interfacial morphology between polymeric matrix and nanoadditives, inducing a better interfacial polarization or valuable crystalline phase [2, 6-10]; the second method focuses on optimizing the processing technique, promoting the reconstruction of the packing morphology of molecular chains as well as the

arrangement of additive nanoparticles [11-12].

Multi-walled/single-walled Carbon nanotubes (MWCNTs/SWCNTs), are treated as the promising candidates for achieving or enhancing functional properties by composing with polymeric matrix owing to the high aspect ratio and low aspect weight, presenting excellent electrical, mechanical and dielectric properties, etc [13-14]. As a cost effective product, the MWCNTs were mostly used in the practical industry for mass production. MWCNTs/polymer nanocomposites with high dielectric constant and good electromechanical properties are attracting more and more attention [12, 15]. A significant improvement of the dielectric performance of the PP/MWCNTs nanocomposites (high dielectric constant and low dielectric loss) was obtained by foaming the polymeric matrix owing to the regular CNTs alignment around the foaming cell [16]. The growing cell during foaming promotes the displacing and rotating behaviors, leading to the transition of isotropic to regular distribution of MWCNTs.

How to obtain good dispersibility [17] and regular alignment of the MWCNTs [11] within the highly viscous polymer matrix melt are the other biggest challenges at present. For example, the electrical conductivity was the most considered property of these polymer/conductive particle composites. A higher percolation threshold value was observed for the composites prepared from melt mixing than that from the solvent solution [18]. The size of the aggregations or clusters and the random networks always largely affects the expected performance [19]. The uniform dispersion of additive reinforcements in polymer matrix and the desirable interfacial adhesion are the key parameters for creating high performance composites. In addition, crystal phase transition should be emphasized simultaneously in the enhancement of dielectric properties [20-21].

Meanwhile, a regular alignment of the carbon tubes, treated as the crystal nuclei, is also helpful to

improve the crystallization phase [22]. Clear β-crystal phase of poly(vinylidene fluoride) (PVDF) was observed at high nanoadditives content [23], which was good at enhancing the dielectric constant. The aggregated clusters, however, were important for promoting the conductive networks within the matrix due to the high aspect ratio of MWCNTs, inducing the typical insulation-conduction transition. By controlling the percolated network structure of functionalized graphene, improved AC conductivity and dielectric properties were ever obtained for polylactic acid nanocomposites [24]. Similarly, significant decreases of the dielectric constant and the conductivity of PVDF/MWCNTs nanocomposites were observed when a tensile strain was applied at room temperature owing to the damage of CNTs clusters or aggregations and the microstructure shift, especially at high loading of MWCNTs [25].

The orientation of the conductive CNTs within polymer matrix was found to be critical in improving the functional performance. How to artificially control the alignment of the CNTs in the host polymers attracts another great interest. The electrospinning technology was the simple and efficient method to obtain highly oriented microstructure of the CNTs, which was well reported in many laboratory works [26-28]. When this requirement was proposed in the practical industry, however, mass production could be the biggest challenge for preparing the nanocomposites.

In this work, highly orientated micro-structure of PP/MWCNTs nanocomposites was prepared by uniaxial die drawing, which was performed at the rubber state of *ca.* 10-20℃ below the melting point of PP. The rheological behavior and dielectric properties of PP/MWCNTs nanocomposites was especially studied through melt compounding for detecting the dispersion or distribution state of MWCNTs. Effects of crystallization morphology and alignment of the molecular chains and MWCNTs were mainly considered as the factors affecting the dielectric performance through DSC,

XRD and dielectric characterizations, etc. It was found that the die drawing process was effective to improving the dielectric performance, decreasing the dielectric constant and also much more significant to decreasing the dielectric loss.

2. Experimental

2.1 Materials

The polymer matrix used in this work was a commercial PP-WB 140HMS from BOREALIS company. It presents a mass density of *ca*. 0.905 g/cm^3 and a melt flow index of *ca*. 1.2 g/(10min). The MWCNTs were purchased from a domestic company (HengQiu, China) with a commercial grade number of HQNANO-MWCNTs-014. These MWCNTs present an internal diameter *ca*. 5-15 nm, an outer diameter above *ca*. 50 nm, a length *ca*. 10-20 μm, a specific surface area *ca*. 40 m^2/g and a mass density *ca*. 2.1 g/cm^3. A coupling agent of organic titanate was used to improve the compatibility between PP matrix and MWCNTs during melt compounding process. PP/MWCNTs nanocomposites with mass contents of MWCNTs *ca*. 0.25, 0.80, 2.0, 5.0 wt% were respectively prepared by using the batching mixer of *PolyLab* (Haake, Germany) under 180℃ and a rotor speeds of 60 rpm. Then these PP/MWCNTs were hot compressed for further experimental analysis.

2.2 Apparatus

Rotational Rheometer

Rheological properties of the PP/MWCNTs melts were measured by an advanced rotational rheometry MCR 501 (Anton-Paar GmbH, Austria) in oscillatory mode with a frequency range of 0.1-100 rad/s at 180℃. The oscillation shear was controlled with 1.0% strain deformation. All measurements were done in air environment utilizing a parallel plate fixture with the diameter equal to 25 mm and a constant 1 mm gap. Circular samples with a 2.0 mm thickness and a 25 mm diameter were hot-compression molded. Complex viscosity and damping factors were obtained as the indexes

of the rheological properties.

Differential Scanning Calorimeter (DSC)

Calorimetric measurements were performed with SHIMADZU DSC-60 instrument (Japan) under a flowing nitrogen atmosphere. Each sample was sealed in a standard aluminum pan. All the measurements were performed with a heating rate of 10℃/min from 80 to 200℃. The tensile-strain effect on the crystalline phase transition can be detected at the first heating process.

Impedance Analyzer

Dielectric properties of MgO/LDPE PNCs were measured using an impedance analyzer system (Agilent 4294A, USA). Plaques, about 1.0 cm^2 in surface area, onto which silver paste had been painted as electrodes, were tested under room temperature. Typical AC applied voltage was 1 V, and frequency ranges from 10^2 to 10^7 Hz. The dielectric constant and the dielectric loss were emphasized for estimating their dielectric and energy storage properties.

X-Ray Diffractometer (XRD)

Investigation of the crystal morphology difference between the die drawn samples and unstretched samples was conducted by an XRD (λ=1.5406 Å, Rigaku D_{MAX}-RB 12kW, Japan) at room temperature. The measured angle ranged from 5-50° (i.e., 2θ=10-100°) with a step width of 0.02°. On considering the orientation effect, wide angle X-ray diffraction (WAXD) measurements were further done for the same samples.

Scanning Electron Microscope (SEM)

The dispersion state of MWCNTs within PP matrix was qualitatively investigated by the scanning electron microscope (SU8010, Hitachi, Japan). The cross-section surface along the drawing direction was adopted for this measurement. Samples were fractured within liquid nitrogen (N_2) and

conductive coating (using Pt) was done for the investigated surface.

3. Results and Discussion

3.1 Rheological behavior

Viscoelastic behavior of the PP/MWCNTs melts were preferentially studied as a fundamental insight to obtain the optimization techniques during the processing step for considering the effect of nanoparticles on the rheological properties. The distribution and the dispersion states of the MWCNTs were found to be critical on the complex viscosity, as shown in fig.1. Compared with the neat PP melt, a significant viscosity reduction of the PP/MWCNTs-0.25 wt% melt was observed at low shear frequency. The complex viscosity decreases from 11,900 to 8, 330 Pa·s with a percentage decrease of *ca.* 30% at low frequency of 0.1 rad/s. Above 0.25 wt%, however, the viscosity increases abruptly with the MWCNTs additive content. A viscosity percentage increase *ca.* 390% of the PP/MWCNTs-5 wt% was observed compared with the pure sample. The decrease or increase of chains entanglement with different MWCNTs should be responsible for these interesting results. With 0.25 wt% MWCNTs addition, a better dispersion state of MWCNTs can be obtained than that with higher concentration. Around these MWCNTs particles, the free volume increases due to the incompatibility and it acts as the “lubricant” role during the molecular chains flowing (fig. 1a). When it comes to a higher particle concentration, however, the aggregation of the nanoparticles is allowed to connect together and this largely blocks the chains movement, leading to a more serious entanglement. The formed network of particle-particle clusters performs the obstacles during the dynamic movements of segments or macrochains during the small oscillation shear measurements. Meanwhile, parts of the molecular chains are adsorbed to particle surface which promotes new

networks and decreases the dynamic activity of molecular chains (fig. 1c). The dispersion state of the MWCNTs within PP matrix was shown in the fig. 2, in which the aggregations of MWCNTs were clearly observed. With a low content loading, several “big aggregation units” were individually unconnected and dispersed randomly.

Similarly, Jain et al [29] and Merkel et al. [30] also suggested that the importance of free volume and interaction between nanofiller and molecular chains could not be neglected for the viscosity variation behavior. The increase of free volume decreases dramatically the internal friction resistance among the molecular chains, leading to apparent decrease of viscosity of the nanocomposite melts. It seems that the generally discussed percolation threshold behavior of the nanoparticles still can be found for the viscosity variation. However, Kim et al. [31] pointed that the percolation threshold was largely determined by a series of intrinsic and external factors, including aspect ratio of CNTs, processing conditions and polymer matrix as well as additives, etc. The effect of the aggregation on the rheological and functional properties is a critically complicated topic on considering the waviness and 3D entanglement of CNTs.

Fig. 1

Fig. 2

Fig. 3

Damping factors, reflecting the viscoelasticity of the polymer melt, was also considered, as shown in fig. 3. It can be found that the composite with 0.25 and 5.0 wt% MWCNTs shows a maximum and a minimum damping factor within the tested frequency range, indicating a viscous dominant and an elastic dominant behavior, respectively. Above 0.25 wt%, the damping factor decreases with the increase of the MWCNTs concentration. This is because apart from the sample with 0.25 wt%

MWCNTs the elastic modulus G' will increase much more with the increasing nanoparticles than that of viscous modulus G''. The elastic behavior will be much more dominant with the increasing of nanoparticles owing to the formation of new networks (as shown in fig. 2). In addition, the MWCNTs component, presenting a much higher G', also enhance the elastic performance of the PP/MWCNTs composites if the effective composite is obtained, as presented in eq. (1).

$$G_c = G_1\varphi_1 + G_2\varphi_2, \quad (1)$$

where G_c is the modulus of composite, G_1, φ_1 and G_2, φ_2 are the moduli and volume fractions of component 1 and 2, respectively. However, the decrease of viscosity is helpful for extrusion or injection process, increasing the melt's flow ability and decreasing the swelling behavior.

3.2 Structure investigation by DSC and XRD

The uniaxial die drawing process was performed with an apparatus in *Polymer IRC Lab* at *University of Bradford* (UK), as shown in fig. 4. It was confirmed that the best temperature for heating the billet was 10-20℃ below its melting temperature [32]. Under this rubber state, the solid phase of PP matrix was extremely stretched. In these experiments, the isotropic PP/MWCNTs samples were heated at *ca*. 140℃ for 5 min by hot air and heated die. Thickness d of the drawing product was controlled by a pair of steel plaques with a certain thickness. The solid billet was then stretched under a controlled drawing speed v. In this work, steel plaques with the thickness of 0.50 and 0.25 mm were adopted for obtaining the drawing ratios of 4.5 and 10, respectively. The drawing processes were performed under 100 and 200 mm/s for considering the effect of drawing speed on the solid phase orientation.

Fig. 4

Fig. 5

Drawing ratio λ, defined by the original thickness d_0 divided by final thickness d, was taken into account as the factor representing the orientation degree induced by this die drawing process, as depicted in eq. (2). This orientated effect was then detected by SEM observation, as shown in fig. 5. It was shown that the aggregated MWCNTs were partly separated and re-arranged along the drawing direction. A fibrous structure was even shown for the samples which were stretched at 200 mm/min and λ=10. It could be supposed that the aggregated MWCNTs clusters were originally surrounded by PP molecular chains and then extensional stress were applied indirectly on these clusters during the die drawing process. This is helpful to promote the dispersion of the aggregated MWCNTs, as shown in fig. 5(a).

$$\lambda = \frac{d_0}{d} \qquad (2)$$

Crystallization morphology of the PP matrix could be significantly changed because this highly stretching process was performed under the rubber state, at which the uniaxial orientation and movement of the rearranged molecular chains were largely maintained after cooling down. Effects of MWCNTs concentration, drawing speed and drawing ratio on the microstructure were considered through the DSC measurements, as shown in fig. 6. Tested samples are commonly named with "MWCNTs content-drawing speed-drawing ratio".

The fact that the intrinsic thermal properties of PP matrix are hardly affected by the introduction of MWCNTs is revealed, but it can still be found that the melting point T_m decreases slightly with the increase of MWCNTs contents (fig. 6a), i.e., the T_m from *ca.* 160.2 (neat, 0%) to 158.2℃ (5 wt%). After die drawing, slight increase of the melting temperature is revealed, even for the samples without MWCNTs addition. It should be noticed that, however, for the billets stretched at high

drawing ratio, a melting plateau including two or more melting peaks are obtained in the DSC patterns, as shown in figs.6b-6c. The melting region is expanded which can be attributed to the breakage of the crystal perfection, causing the single melting point changing into a wide melting region. The conformational restrictions in the amorphous phase are broken down and then come to the secondary crystallization. The expansion of the melting peak increases the melting enthalpy ΔH_m, which is generally used to calculate the crystallinity by dividing the ideal enthalpy ΔH_0 of a 100% crystalline PP.

Fig. 6

Fig. 7

Fig. 8

In addition, the higher drawing ratio is found to be more helpful to increase the second melting temperature which was also implied in the DSC measurements. As discussed above, the original crystallites could be broken down during die drawing and new crystallites can be reformed under the rubber state temperature. This is helpful to promote the size growth of the crystallites. The XRD measurements were carried out for supporting this conjecture, as shown in fig. 7. Intensities of the dominant α phase at (110), (040), (130) and (060) increase simultaneously after drawing, but the intensities at (110) and (130) increase much more. The orientation behavior of the microstructure was further studied by WAXD measurements, as shown in fig. 8. It is found that significant orientation is observed for the stretched samples while it is hardly found for the unstretched sample. And in common sense, higher orientation degree is positively revealed from the samples with a higher drawing ratio.

3.3 Dielectric performance

The real ε' and imaginary ε'' parts of the relative dielectric constant can be calculated as follows [33]:

$$\varepsilon' = \frac{C_p d}{A\varepsilon_0} \quad , \qquad (3)$$

$$\varepsilon'' = \frac{d}{A\omega\varepsilon_0 R_p} \quad , \qquad (4)$$

$$\tan\delta = \frac{\varepsilon''}{\varepsilon'} \quad , \qquad (5)$$

where d is the specimen thickness, A is the area of contact surface, ε_0 is the free-space permittivity, and R_p=1/G is the equivalent parallel resistance. The generally speaking dielectric constant ε is related to the real part ε', i.e., ε'=ε, which is a measure of how much energy can be stored in the material upon the application of external electric field. Dielectric loss tanδ, presenting the energy loss, includes Ohmic loss and polarization loss.

The increased dielectric constant ε of the polymer nanocomposites by introducing conductive particles is based on the enhancement of interfacial polarization [3]. As shown in fig. 9, both the ε and tanδ increase with the loading of MWCNTs, which was also revealed in the other literatures [9, 23]. The introduction of MWCNTs effectively increases the ε, especially near the percolation threshold of MWCNTs concentration (between 2 and 5 wt%). Dielectric loss tanδ, however, also increases simultaneously, causing large energy consumption. But the effects of drawing speed and drawing ratio cannot be neglected.

With a high drawing ratio and a high drawing speed, both ε and tanδ decrease significantly. The dielectric loss of the stretched samples was as low as the neat PP when the loading of MWCNTs was no higher than 2 wt%, which is important for dielectric applications. Compared with the pure PP, for example, ε of the samples with 2 wt% MWCNTs present a percentage increase of *ca.* 26.4% at v=100 mm/s and λ=4.5, and a percentage increase *ca*. 29.2% of the ε at v=200 mm/s and λ=10. The tanδ of

all the tested samples with 2 wt% MWCNTs are almost the same, ranging in 0.005-0.01. As to the sample with 5 wt% MWCNTs, the ε are 67.7 and 38.0 with λ=4.5 at v=100 mm/s and v=200 mm/s, respectively. When the drawing ratio increases to 10, the ε are 9.7 and 8.2 at v=100 mm/s and v=200 mm/s, decreasing by no more than one order of magnitude, respectively. The tanδ, however, are 6.9 and 27.6 with λ=4.5 at v=100 mm/s and v=200 mm/s and are 0.68 and 0.25 with λ=10 at v=100 mm/s and v=200 mm/s, respectively. About 1-2 order of magnitude decrease is revealed. This suggests that the highly orientation of the microstructure not only decreases the dielectric constant but also decreases the dielectric loss more significantly. The fact that the decrease of tanδ is good at exploring practical applications of this PP/MWCNTs nanocomposite is generally accepted.

Fig. 9

The dielectric constant increase ratio r, used to estimate the relationship between orientation degree and dielectric performance, was defined by eq. (6) as

$$r = \frac{\varepsilon_s}{\varepsilon_p}, \qquad (6)$$

where ε_s is the dielectric constants of the stretched samples at a certain frequency, ε_p is the dielectric constant of the pure PP (e.g. ε_p=2.38 and tanδ =0.01 at 1 kHz). An overview of the enhancement of ε is given in fig. 10, in which the increase ratio r was calculated at the certain frequency of 1 kHz.

Fig. 10

Fig. 11

The dielectric constant increases with increasing of MWCNTs content owing to the enhancement of

electronic displacement polarization. Significant decrease of ε_s, however, is also found compared with the ε_p. MWCNTs are dispersed within the PP matrix as individual tubes or aggregations in random direction and construction of the conductive networks could be obtained due to the clusters, as previously shown in fig. 2. The abrupt increase of ε_0 should be contributed to this successful construction of conductive networks, simultaneously introduced by plenty of free electrons. But most of the networks are damaged during the uniaxial drawing, consequently decreasing the electronic displacement polarization effect and then reducing the dielectric constant. Meanwhile, the solid phase orientation also confines the movement of molecular chains, causing a decrease of the polarization effect of dipole moment orientation. This conjecture can be further confirmed by the resistivity measurement, as shown in fig. 11. The conductivity of PP/MWCNTs-5 wt% composites was taken as an example. Comparing with the unstretched sample, the volume conductivity of drawn billets is obviously reduced by the die drawing process. Although a higher orientation degree and a more negative aggregated dispersion of MWCNTs were obtained at drawing ratio λ=10, however, its volume resistivity of PP/MWCNTs-5 wt% is lower than that at λ=4.5. This is because the network connection between MWCNTs was broken down along the drawing direction but it could be bridged again along the thickness direction, as schematically shown in fig. 5(b). It still can be concluded that, therefore, the higher orientation degree of the microstructures of both MWCNTs clusters and networks is, the lower ε_s could be obtained. Well dispersed MWCNTs will remarkably improve the dielectric performance for its polymeric nanocomposite. Highly orientated solid phase not only changes the crystallization behavior of the polymer matrix, but also changed the morphology of MWCNTs clusters or dispersion state.

4. Conclusions and perspective

Dependence of the viscoelastic behavior and dielectric dependence on the MWCNTs concentration as well as the orientation effects of the microstructures were investigated in the present work. A low MWCNTs concentration was found to be helpful to decrease the viscosity of the composite melt, increasing the flow ability and the viscous behavior due to the “lubricant” effect and the increase of the free volume. Solid phase orientation was obtained through the die drawing process performed at rubber state temperature *ca.* 140℃ below the PP melting point. A wide melting plateau was clearly revealed from the DSC measurement, indicating a damage of the crystal perfection and a second generation of new crystallite. The effect of crystallization morphology transition on dielectric properties was found to be negative to enhance the polarization property of the PP/MWCNTs, leading to a small amplitude decrease of the dielectric constant. It was suggested that, however, the aggregated MWCNTs clusters or conductive networks were largely broken down by the highly uniaxial tensile, remarkably decreasing the electronic displacement polarization effect and then decreasing dielectric constant as well as dielectric loss.

Acknowledgements

The authors wish to thank the financial support of National Natural Science Foundation of China (NSFC51473018), China Postdoctoral Science Foundation (2015M570928) and the Fundamental Research Funds for the Central Universities (FRF-TP-14-013A1).

References

[1] Dang Z. M.; Yuan J. K.; Zha J. W.; Zhou T. Z.; Li S. T.; Hu G. H. Prog. Mater. Sci. 2012, 57: 660–723.

[2] Selvi M.; Vengatesan M. R.; Prabunathan P.; Song J. K.; Alagar M. Appl. Phys. Lett., 2013, 103: 152902.

[3] Kim J. Y.; Kim T. Y.; Suk J. W.; Chou H.; Jang J. H.; Lee J. H.; Kholmanov I. N.; Akinwande D.; Ruoff R. S. Small, 2014, 10: 3405–3411.

[4] Arjmand M.; Sundararaj U. Polym. Eng. Sci., 2015, 55: 173–179.

[5] Wang Z.; Zhao G. L. J. Mater. Chem. C, 2014, 2: 9406–9411.

[6] da Silva A. B.; Arjmand M.; Sundararaj U.; Bretas R. E. S. Polym. 2014, 55: 226–234.

[7] Sharma M.; Madras G.; Bose S. Phys. Chem. Chem. Phys., 2014, 16: 2693–2704.

[8] Qiang Z. X.; Liang G. Z.; Gu A. J.; Yuan L. J. Nanopart. Res., 2014, 16: 2391–2409.

[9] Long Y.; Pu Z. J.; Huang X.; Jia K.; Liu X. B. J. Polym. Res., 2014, 21: 525–534.

[10] Guo X. S.; Yu D. M.; Wu J. S.; Min C.; Guo R. N. Polym. Eng. Sci., 2013, 53: 370–377.

[11] Zhang W.; Ning N. Y.; Gao Y.; Xu F.; Fu Q. Compos. Sci. Technol., 2013, 83: 47–53.

[12] Jouni M.; Boiteus G.; Massardier V. Polym. Adv. Technol., 2013, 24: 909–915.

[13] Xu H.; Anlage S. M.; Hu L.; Gruner G. Appl. Phys. Lett., 2007, 90: 183119.

[14] Li C.; Thostenson E. T.; Chou T. W. Compos. Sci. Technol., 2008, 68: 1227–1249.

[15] Zhang S. H.; Zhang N. Y.; Huang C.; Ren K. L.; Zhang Q. M. Adv. Mater., 2005, 17:1897–1901.

[16] Ameli A.; Nofar M.; Park C.B.; Pötschke P.; Rizvi G. Carbon, 2014, 71: 206–217.

[17] de Luna M. S.; Pellegrino L.; Daghetta M.; Mazzocchia C. V.; Acierno D.; Filippone G. Compos. Sci. Technol., 2013, 85: 17–22.

[18] Thomassin J. M.; Trifkovic M.; Alkarmo W.; Detrembleur C.; Jérôme C.; Macosko C. Macromolecules, 2014, 47: 2149–2155.

[19] de Vivo B.; Lamberti P.; Spinelli G.; Tucci V. J. Appl. Phys., 2014, 115: 154311.

[20] Sharma M.; Madras G.; Bose S. Phys. Chem. Chem. Phys., 2014, 16: 2693–2704.

[21] Zheng P. L.; Pu Z. J.; Yang W.; Shen S. Z.; Jia K.; Liu X. B. J. Mater. Sci. Mater. Electron., 2014, 25: 3833–3839.

[22] Baji A.; Mai Y. W.; Abtahi M.; Wongm S. C.; Liu Y.; Li Q. Compos. Sci.Technol., 2013, 88: 1–8.

[23] Tiberio A. E.; José C. C.; Alejandro S.; Amelia L. Colloid Polym. Sci., 2014, 292: 1989–1998.

[24] Fu Y.; Liu L. S.; Zhang J. W. ACS Appl. Mater. Interfaces, 2014, 6: 14069–14075.

[25] Dang Z. M.; Yao S. H.; Xu H. P. Appl. Phys. Lett., 2007, 90: 012907.

[26] Xu W. H.; Ding Y. C.; Jiang S. H.; Zhu J.; Ye W.; Shen Y. L.; Hou H. Q. Eur. Polym. J., 2014, 59: 129–135.

[27] Hou H.; Ge J. J.; Zeng J.; Li Q.; Reneker D. H.; Greiner A.; Cheng S. Z. D.; Chem. Mater., 2005, 17: 967–973.

[28] Ning N. Y.; Bai X.; Yang D.; Zhang L. Q.; Lu Y. L.; Nishi T.; Tian M. RSC Adv., 2014, 4: 4543–4551.

[29] Jain S.; Goossens J. P.; Peters G. M.; van Duin M.; Lamstra P. Soft Matter, 2008, 4(9): 1848-1854.

[30] Merkel T. C.; Freeman B. D.; Spontak R. J.; He Z.; Pinnau I.; Meakin P.; Hill A. Science, 2002, 296(5567): 519-522.

[31] Li J.; Ma P. C.; Chow W. S.; To C. K.; Tang B. Z.; Kim J. K. Adv. Funct. Mater., 2007, 17, 3207-3215.

[32] Coates P. D.; Fin C. R.; Ward I. M.; Glen T. Sci. China Chem., 2013, 56: 1017–1028.

[33] Osayuki O.; Marianna K.; Ribal G. S.; Aristides D. Macromol. Mater. Eng., 2015, 300, 448–457.

Figure captions

Fig.1 Complex viscosity of the PP/MWCNTs nanocomposites with varied MWCNTs loading.

Fig.2 SEM observations of the MWCNTs dispersion state at different loadings.

Fig.3 Damping behavior of the PP/MWCNTs nanocomposites with varied MWCNTs loading.

Fig.4 Schematics of the (a) die drawing and (b) experimental apparatus.

Fig.5 Comparison of the dispersion state of MWCNTs at different drawing ratios: (a) SEM observation of the morphology of the billets before and after solid phase orientation at different drawing speeds and drawing ratios. Samples with 5 wt% MWCNTs addition were adopted; (2) Schematics of the conductive networks of the MWCNTs in the PP matrix.

Fig. 6 DSC patterns of PP and PP/MWCNTs nanocomposites with different MWCNTs content (a), drawing ratios and speeds (b, c, d).

Fig. 7 XRD patterns of the (a) pure PP and (b) PP/MWCNTs (5 wt%).

Fig. 8 WAXD patterns of the (a) pure PP and (b) PP/MWCNTs (5 wt%).

Fig. 9 Dielectric performance of the PP or PP/MWCNTs drawn at: 100 mm/s (a) and 200 mm/s (b).

Fig. 10 Dielectric constant ratios of unstretched and stretched PP/MWCNTs at 1 kHz.

Fig.11 Volume resistivity of the PP/MWCNTs-5% at different drawing ratios and drawing speeds.

Figures

Fig. 1

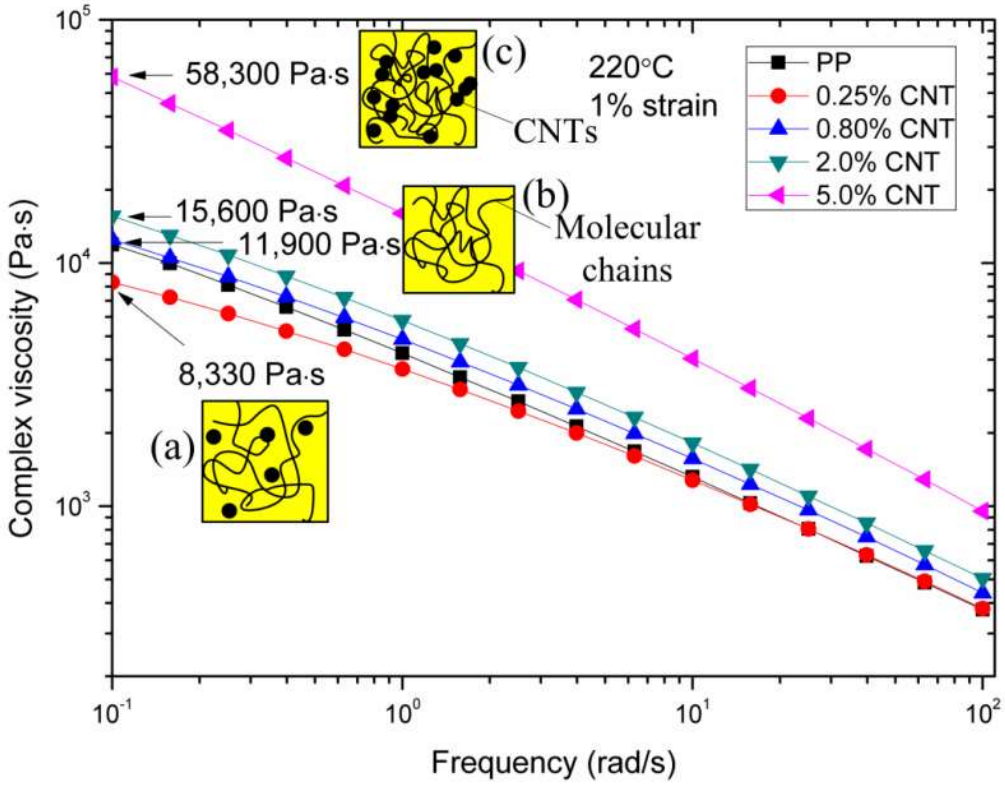

Fig. 2

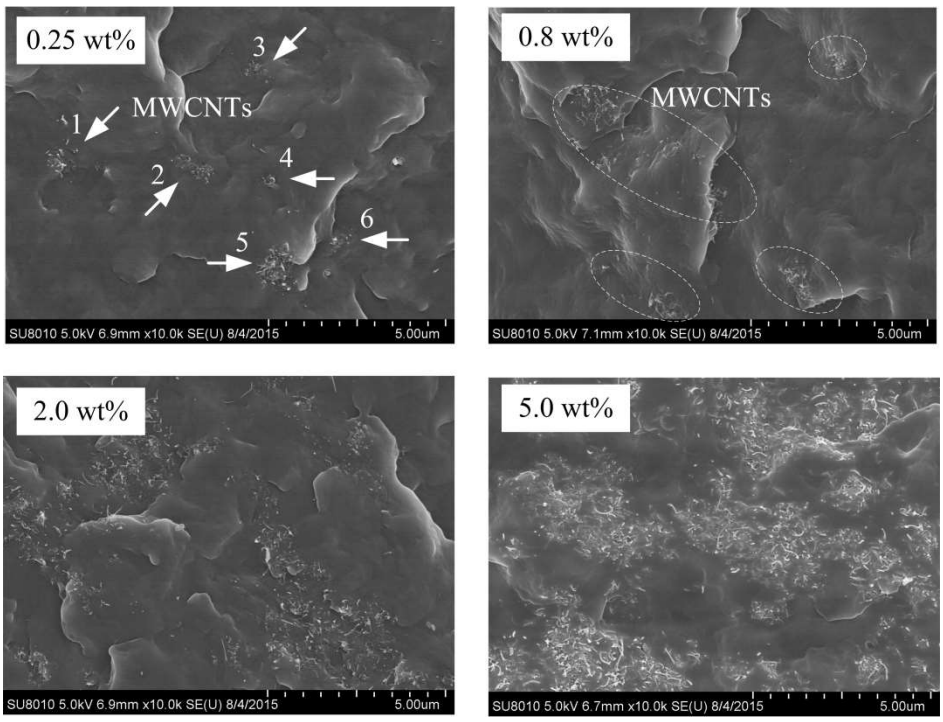

Fig. 3

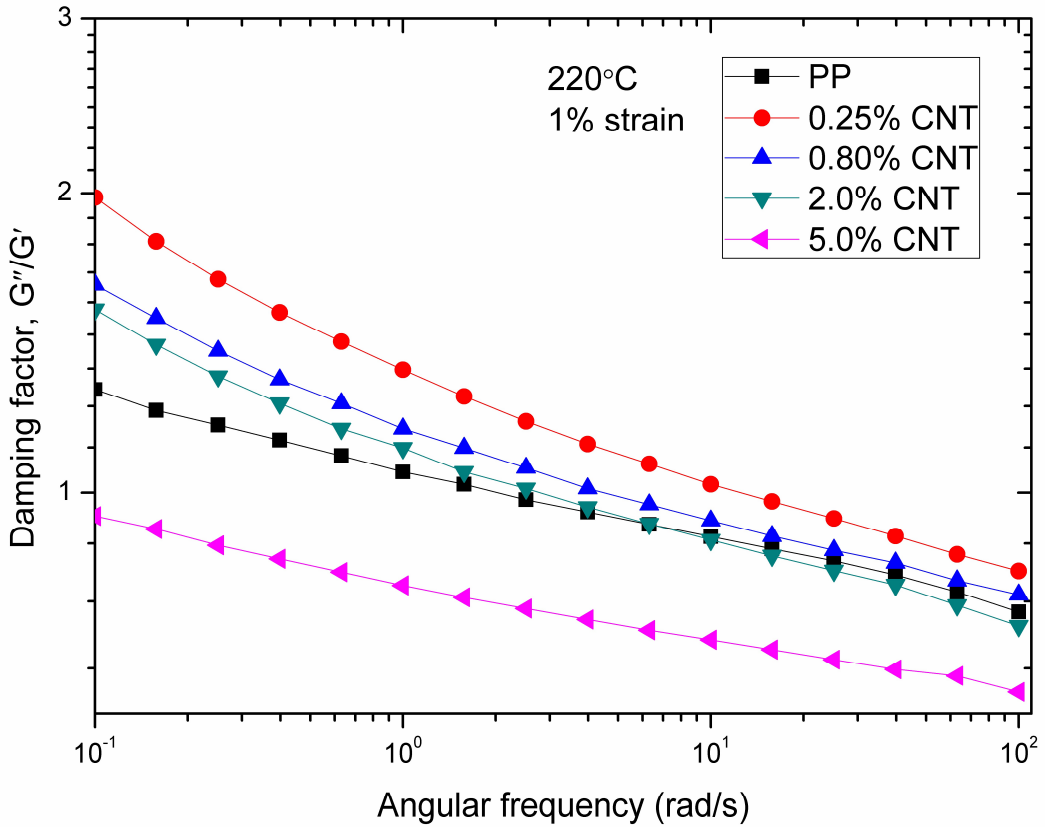
220°C
1% strain
PP
0.25% CNT
0.80% CNT
2.0% CNT
5.0% CNT
Damping factor, G″/G′
Angular frequency (rad/s)
3
2
1
10-1
100
101
102

Fig. 4

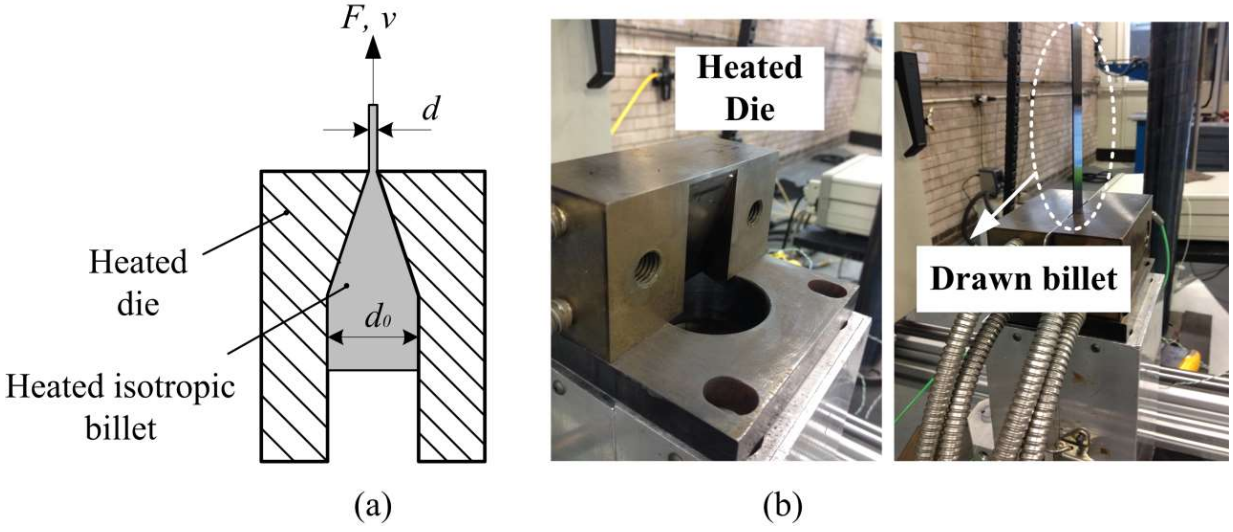
F, v
d
Heated
die
d0
Heated isotropic
billet
(a)
Heated
Die
Drawn billet
(b)

Fig. 5

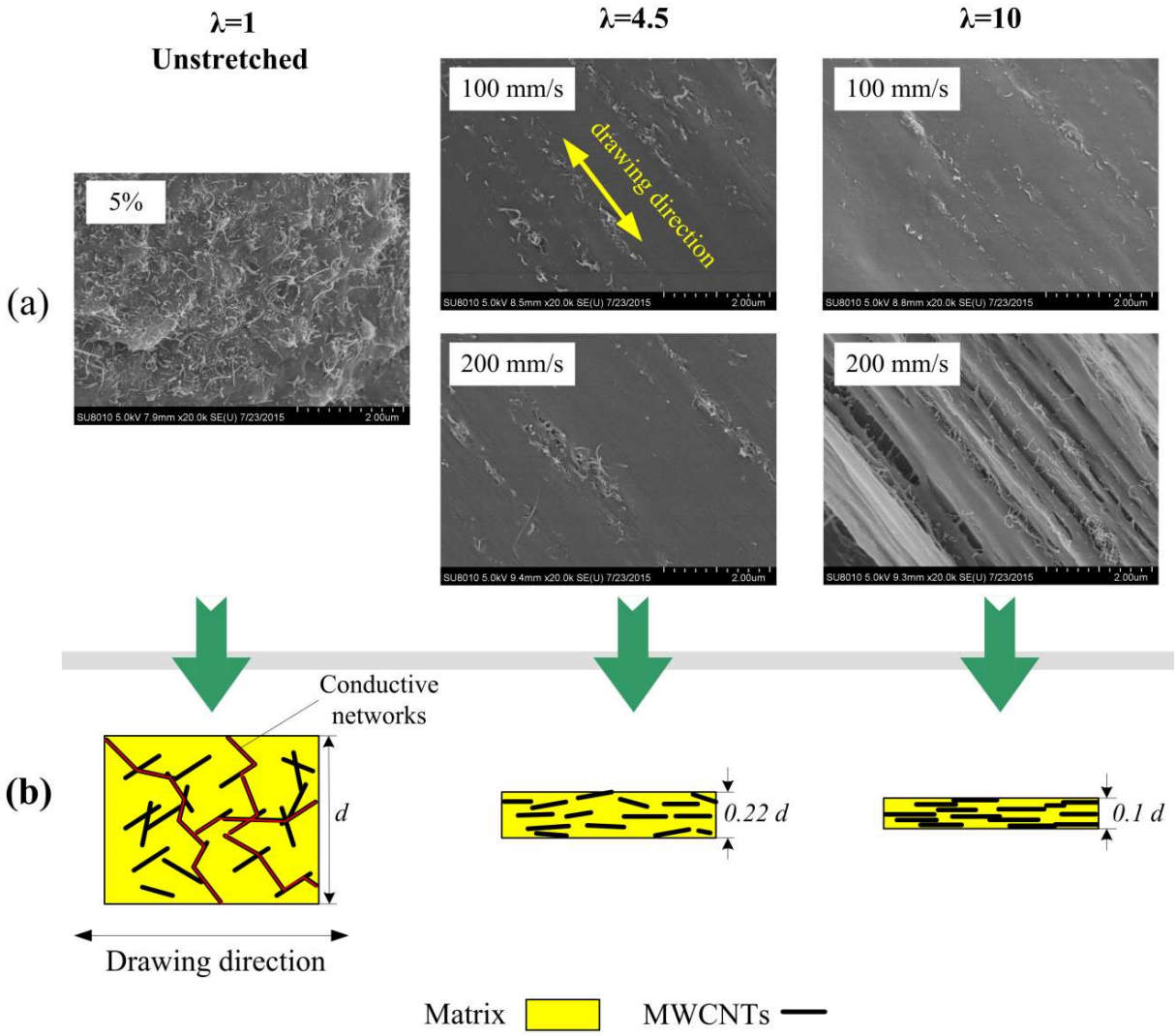
λ=1
Unstretched
λ=4.5
λ=10
(a)
5%
100 mm/s
drawing direction
100 mm/s
200 mm/s
200 mm/s
(b)
Conductive networks
d
0.22 d
0.1 d
Drawing direction
Matrix
MWCNTs

Fig. 6

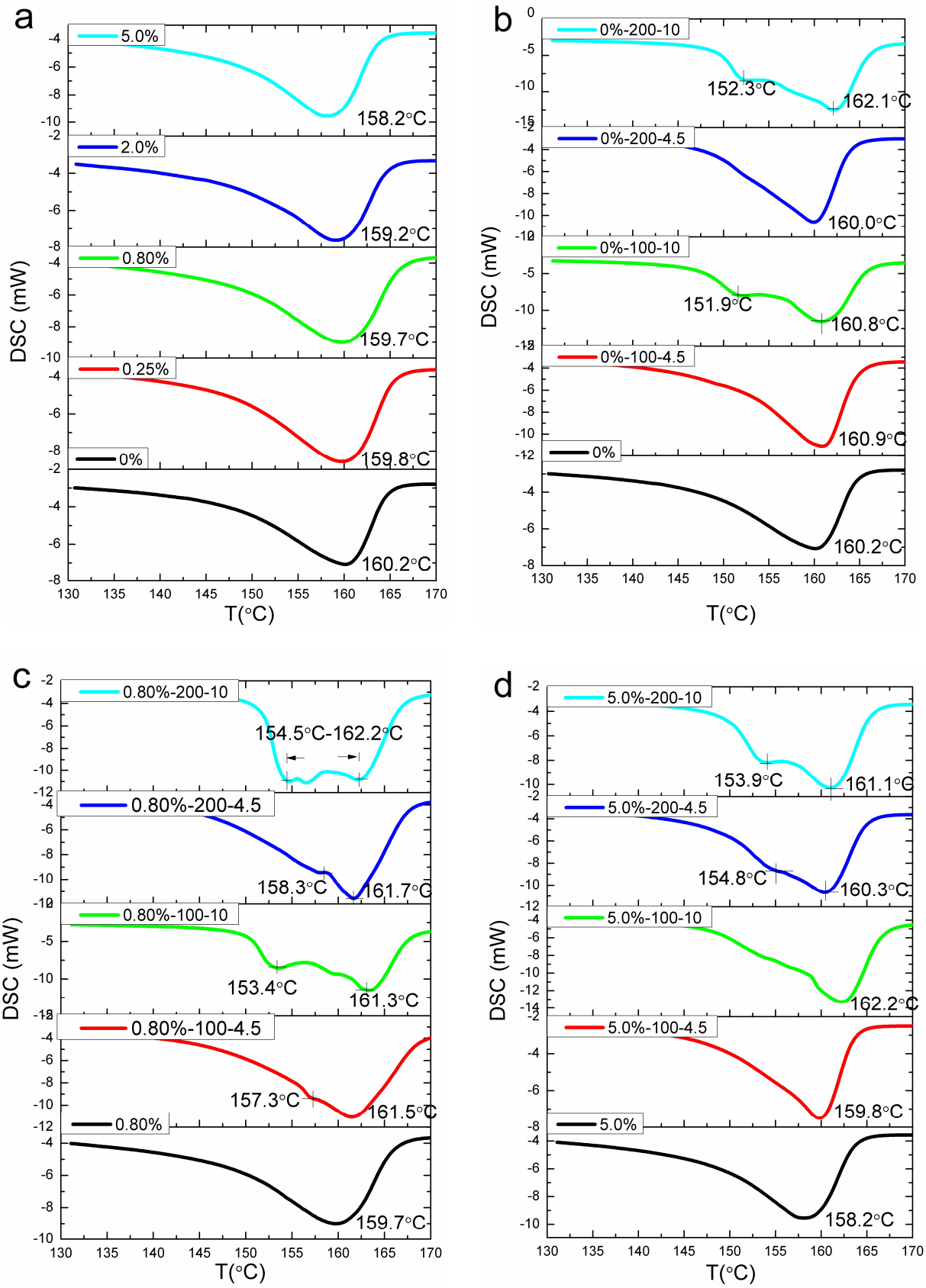
a
5.0%
158.2°C
2.0%
159.2°C
0.80%
159.7°C
0.25%
159.8°C
0%
160.2°C
DSC (mW)
T(°C)
b
0%-200-10
152.3°C
162.1°C
0%-200-4.5
160.0°C
0%-100-10
151.9°C
160.8°C
0%-100-4.5
160.9°C
0%
160.2°C
DSC (mW)
T(°C)
c
0.80%-200-10
154.5°C-162.2°C
0.80%-200-4.5
158.3°C
161.7°C
0.80%-100-10
153.4°C
161.3°C
0.80%-100-4.5
157.3°C
161.5°C
0.80%
159.7°C
DSC (mW)
T(°C)
d
5.0%-200-10
153.9°C
161.1°C
5.0%-200-4.5
154.8°C
160.3°C
5.0%-100-10
162.2°C
5.0%-100-4.5
159.8°C
5.0%
158.2°C
DSC (mW)
T(°C)

Fig. 7

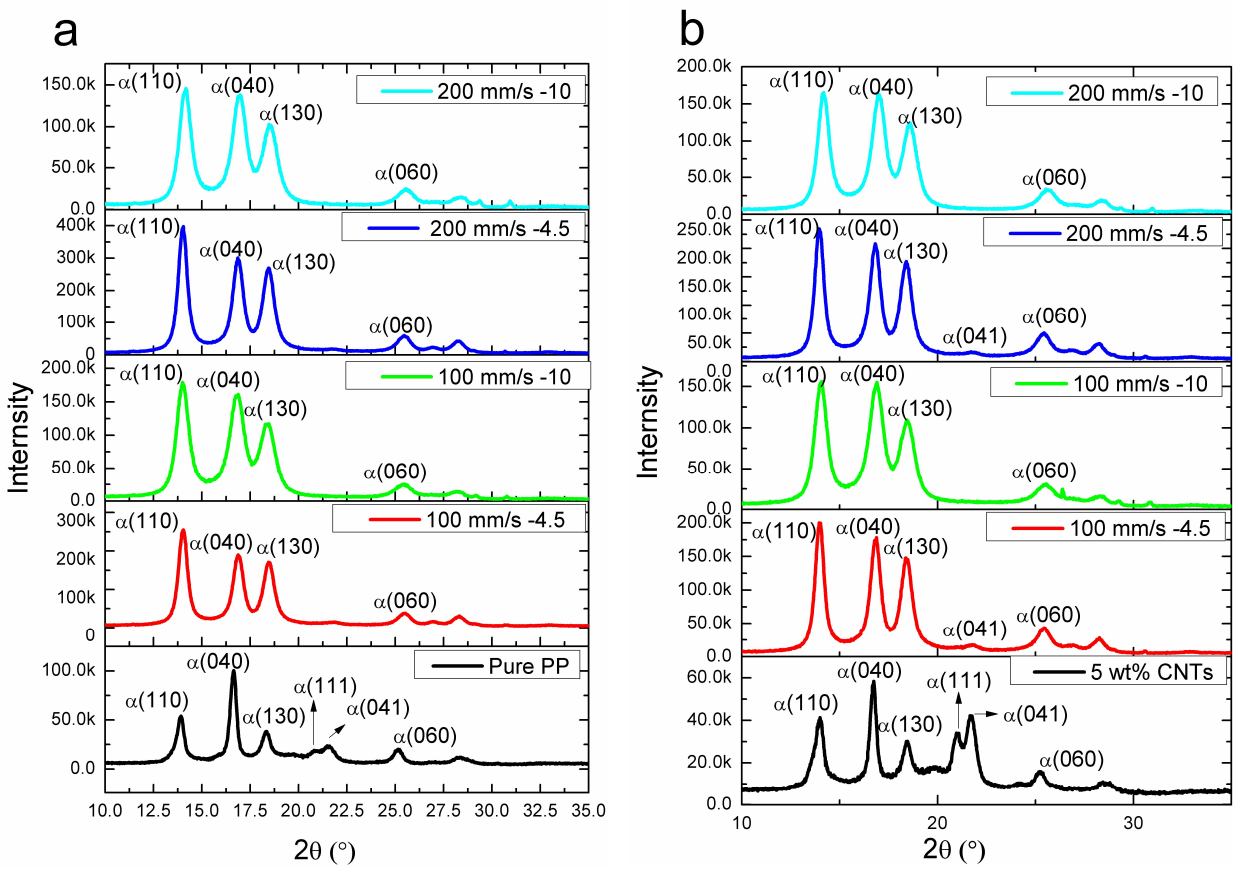
a
b
Internsity
2θ (°)
200 mm/s -10
200 mm/s -4.5
100 mm/s -10
100 mm/s -4.5
Pure PP
5 wt% CNTs
α(110)
α(040)
α(130)
α(111)
α(041)
α(060)

Fig. 8

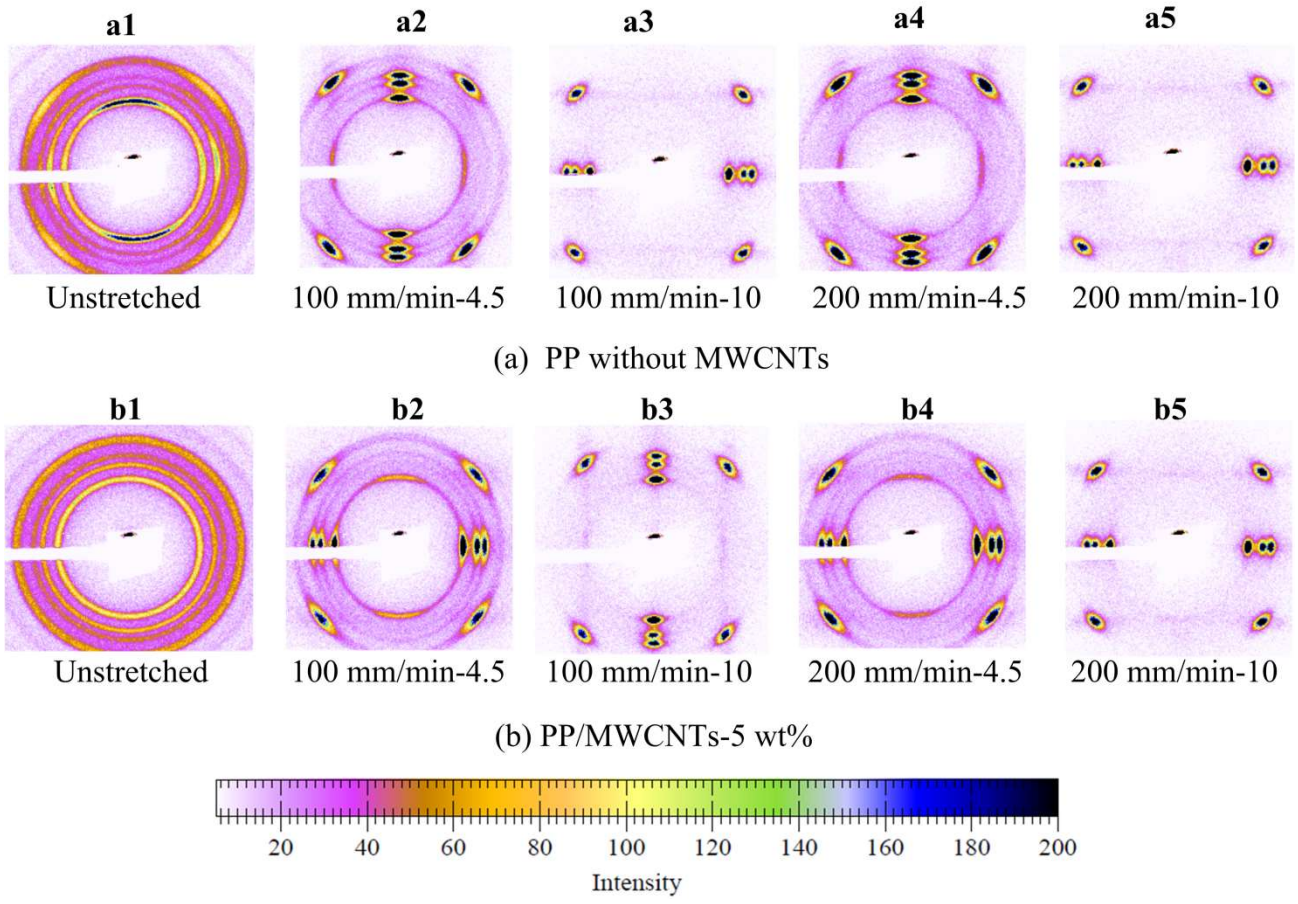
a1
a2
a3
a4
a5
Unstretched
100 mm/min-4.5
100 mm/min-10
200 mm/min-4.5
200 mm/min-10
(a) PP without MWCNTs
b1
b2
b3
b4
b5
Unstretched
100 mm/min-4.5
100 mm/min-10
200 mm/min-4.5
200 mm/min-10
(b) PP/MWCNTs-5 wt%
20
40
60
80
100
120
140
160
180
200
Intensity

Fig. 9

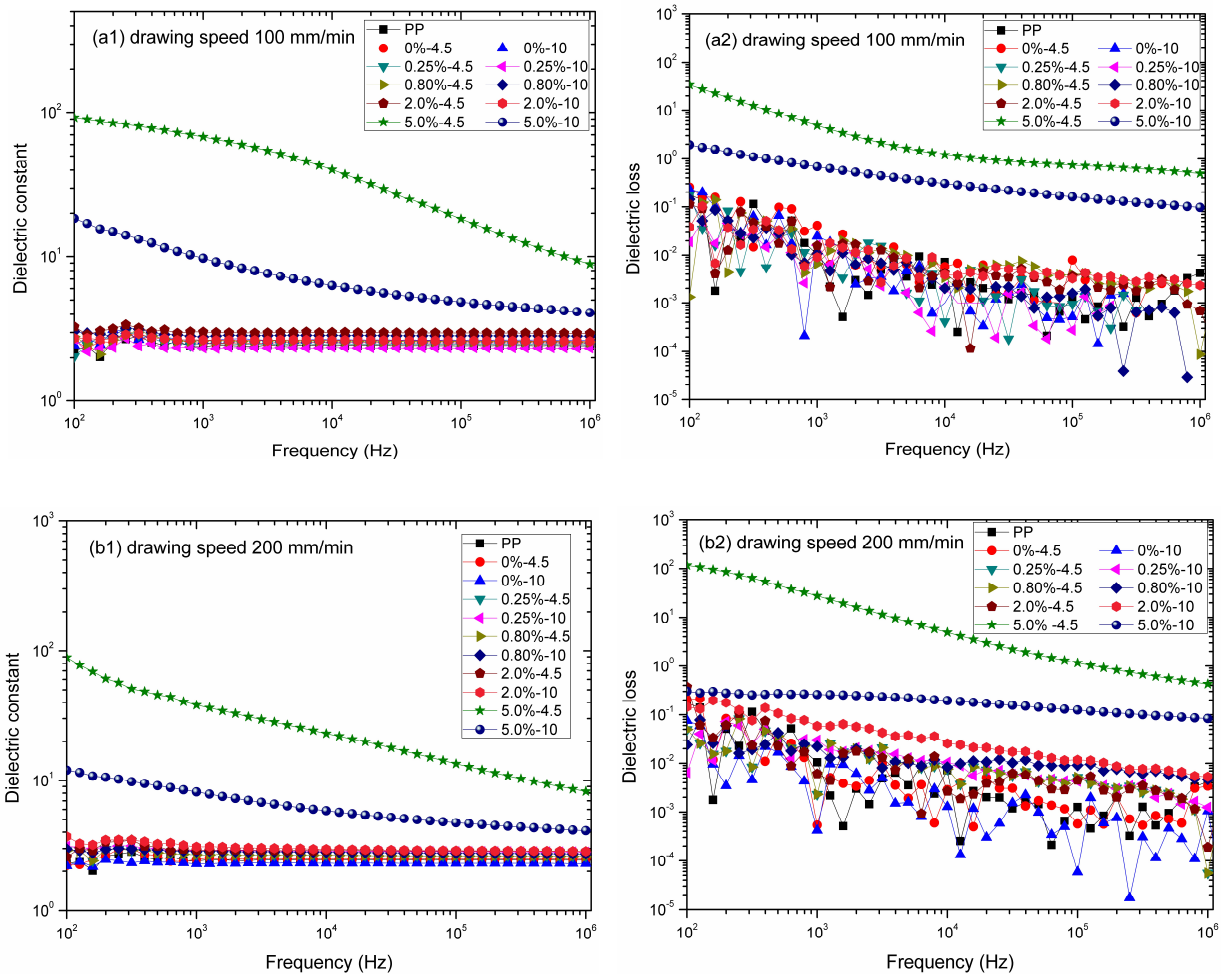
(a1) drawing speed 100 mm/min
(a2) drawing speed 100 mm/min
(b1) drawing speed 200 mm/min
(b2) drawing speed 200 mm/min
PP
0%-4.5
0%-10
0.25%-4.5
0.25%-10
0.80%-4.5
0.80%-10
2.0%-4.5
2.0%-10
5.0%-4.5
5.0%-10
5.0% -4.5
Dielectric constant
Dielectric loss
Frequency (Hz)

Fig. 10

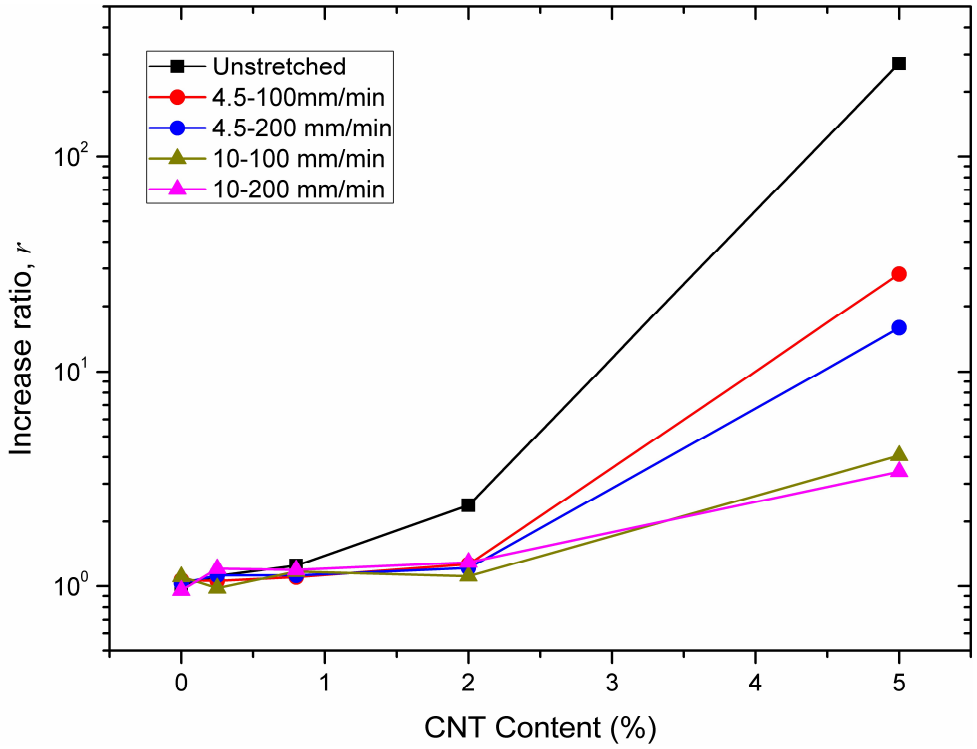
Unstretched
4.5-100mm/min
4.5-200 mm/min
10-100 mm/min
10-200 mm/min
Increase ratio, r
CNT Content (%)

Fig. 11

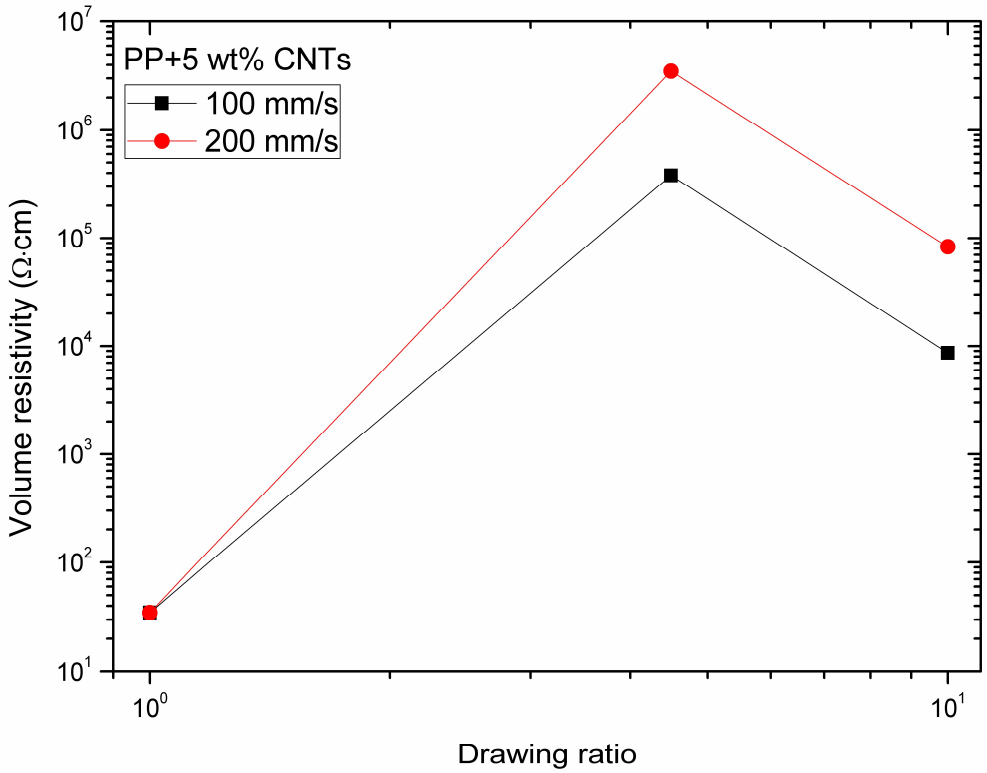
PP+5 wt% CNTs
100 mm/s
200 mm/s
Volume resistivity (Ω·cm)
Drawing ratio